Experimentally Validated Modelling of Electromechanical Dynamics on Local Magnetic Actuation System for Abdominal Surgery

Florence Leong[1], Alireza Mohammadi[1], Ying Tan[1], Dhan Thiruchelvam[2], Pietro Valdastri[3], Denny Oetomo[1]

[1] Dept of Mechanical Engineering, University of Melbourne, Australia
[2] St Vincent's Dept of Surgery, University of Melbourne, Australia
[3] School of Electronic and Electrical Engineering, University of Leeds, UK
fleong@student.unimelb.edu.au, doetomo@unimelb.edu.au

Abstract

This paper builds on the emerging idea of the Local Magnetic Actuation (LMA) system for robotic abdominal surgery, that allows the rigid linkages for the surgical manipulator in minimally invasive surgery to be replaced by magnetic linkages across the abdominal wall. In this paper, the equation of motion for the internal unit, inserted into the abdominal cavity, is derived in all 6 spatial degrees of freedom. Firstly, the resultant magnetic field at the location of the rotor, generated by a source at an arbitrary displacement from the rotor, is modelled. Secondly, the model of the wrench acting on the internal rotor unit generated by the magnetic flux linkage between the above mentioned field and that of the permanent magnet rotor is derived (by Newton Euler approach). The contributions of multiple sources of magnetic field on the forces and moments acting on the internal rotor unit are taken into account by the principle of superposition. The paper then carries out system identification on an experimental set up. Numerical computational and experimental validations were carried out on the magnetic field model and magnetic-torque model, as well as confirming the validity of the principle of superposition for our problem.

Keywords:
Local magnetic actuation (LMA), Electromagnetic actuation, abdominal surgery,robot assisted surgery, minimally invasive surgery.

1 Introduction

Local Magnetic Actuation [Di Natali *et al.*, 2015] techniques have been investigated recently as a variant to the conventional minimally invasive surgical (MIS) [Richardson *et al.*, 2000] approach to improve the dexterity and mobility of the surgical robotic manipulators while maintaining the minimum level of surgical trauma. This improvement is done by removing the need for rigid link transmission to the surgical manipulator inserted through the incision hole. Currently targeted at abdominal surgeries, the technique allows a surgical manipulator to be completely inserted into the insufflated abdominal cavity and its motion regulated through the use of magnetic linkages between external stator units and the internal rotors. The absence of a rigid link transmission means that the manipulator is no longer constrained by the location of the incision point. The entire surgical manipulator is therefore completely inserted into the abdominal cavity and is free to move to cover different quadrants of the abdomen. The incision hole therefore now serve only as the entrance and exit point for the internal units. As such, it is envisaged that this approach will bring about significant improvement to the dexterity and mobility of a surgical robot, reaching different quadrants of the abdominal cavity, while maintaining the minimal level of surgical trauma achieved by the current state-of-the-art MIS systems. The summary of the technique is depicted in Figure 1.

Review of the magnetic-based surgical manipulators was presented in [Leong *et al.*, 2016]. The use of magnetic coupling to address the need to remove rigid mechanical link in laparoscopic devices was experimented in the form of the magnetic anchoring and guidance (MAGS) surgical devices [Cadeddu *et al.*, 2009], [Park *et al.*, 2007] which can be completely deployed intra-abdominally via a single incision point. These internal devices statically held surgical instruments such as tissue retractor and camera onto the inside wall of the abdominal cavity with the help of permanent magnet anchors. These systems are generally not actuated. A surgical manipulator actuated by on board DC micromotors [Tortora *et al.*, 2013] was anchored with the MAGS and was demonstrated to provide a maximum pulling force of 1.53N with a resulting dimension that could be inserted through a 5mm incision. While improved dexterity was demonstrated, the resulting torque was insufficient for surgical procedures working with high payload (e.g. a liver tissue retraction task is typically rated at 5N load) [Leong *et al.*, 2016] and the space constraint of the abdominal cavity means that there is little room for future improvements.

To allow a more powerful (thus larger) system, actuation

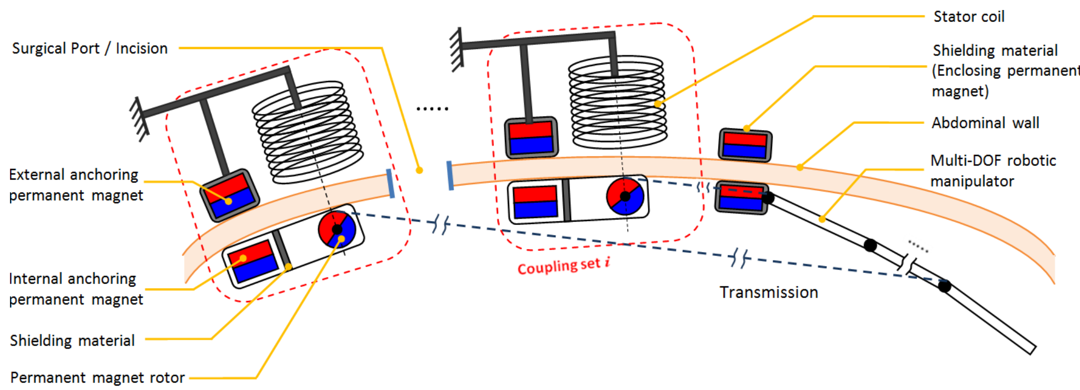

Figure 1: Schematic representation of the simplified LEMA system involving a single coil-single rotor model where torque at permanent magnet rotor, *i* is transmitted to the robotic manipulator through an appropriately designed mechanism, e.g. cable.

external to the abdominal cavity was studied, thus alleviating the space constraint. This was attempted by externally generating the actuation magnetic field using a magnetic resonance imaging (MRI) machine [Vartholomeos *et al.*, 2013] to drive needle insertion for neurosurgery, using multiple electromagnetic coils to regulate for the pose of a micro robot for eye surgery [Kummer *et al.*, 2010], or by the use of a external magnet placed around the patient to navigate magnetically-driven internal surgical devices (e.g. wireless capsule endoscopes) [Munoz *et al.*, 2015], [Carpi *et al.*, 2009]. These methods however, are geared towards manipulating lower number of independent degrees-of-freedom (DOFs) in the mechanisms, as it produces a uniform field across the entire workspace.

Instead of a uniform field across the workspace, Local Magnetic Actuation (LMA) [Di Natali *et al.*, 2015] approaches exploit localised magnetic coupling between an external source of actuation and an internal rotor across the abdominal wall. The localised nature allows for multiple of such stator-rotor pairs to be deployed, thus allowing (ideally) multiple independent degrees-of-freedom (DOFs) of actuation within the workspace, which is crucial in the application of robotic surgery. The multiple DOF LMA implemented using permanent magnet stator and rotor was shown to effectively actuate a 2DOF continuum arm robotic camera system [Hang *et al.*, 2015] and a 3DOF surgical manipulator [Mohammadi *et al.*, 2015]. Electromagnetic coils were investigated for the LMA approach for a more direct method of regulating the resulting magnetic field. To differentiate this approach from the permanent magnet based LMA, the term localised electromagnetic system (LEMA) is used in this paper. A LEMA system with two stator coils was presented in [Mohammadi *et al.*, 2015][Mohammadi *et al.*, 2015] which demonstrated empirically the robustness of the system with some uncertainties, e.g. coupling misalignment of the internal unit deployment and the variation in abdominal wall thickness. The model presented only involved the dynamics of the internal rotor unit in the generalised coordinate (in the axis of rotation of the rotor). Practical uncertainties, resulting from simplifying assumptions such as one that assumes all other degrees of freedom are perfectly rigid, or the disturbances caused by the magnetic fields from the neighbouring stator-rotor pairs, were not considered and handled by feedback controller.

The LEMA system setup in the abdominal surgery environment is illustrated in Figure 1, where multiple stator - rotor units (electromagnetic stator coil and permanent magnet rotor) of LEMA configuration are utilised to drive a surgical robotic manipulator with corresponding number of DOFs. A single incision is used as the entrance and exit point of the internal units to the abdominal cavity. Each DOF on the robotic manipulator is actuated by a LEMA rotor, through some transmission mechanism, e.g. cable. The external portion of the LEMA system, consisting of the electromagnetic stator coils and the external permanent magnet anchor, can be attached rigidly to a platform, hence providing stable operation.

In this paper, the model for the dynamics of the LEMA system is derived and presented. More specifically, the models for (1) a magnetic field generated by an electromagnetic coil at an arbitrary location representing the centre of the internal rotor unit and (2) the 6 DOF force and moment (wrench) generated by the magnetic flux linkage between the resultant field at the location of the rotor and that of the permanent magnet internal rotor, as presented in Section 2. This provides a general case model that would account for any magnetic field acting on the rotor, generated by an external set of coil(s) for the intended actuation, as well as any other fields generated by other magnetic sources, such as the anchoring magnets, other rotors and stators. Note that the model takes into account not only the generated rotor torque about its axis of rotation, but also the other 5 degrees of freedom of interaction wrench which were ideally assumed to be rigid. In practice, however, these components will comprise non-rigid systems, such as the viscoelastic nature of the abdominal wall that the system is magnetically anchored onto. The model also allows other non-systematic uncertainties, such as the error in the estimation of abdominal wall thickness and the misalignment in the placement of the rotor relative to the external stator unit, to be taken into account. Section 3 describes the experimental set up while Section 4 describes the system identification process. Section 5 presents the result of the numerical and experimental validation exercise. T Additionally, the paper utilises *Principle of Superposition* to allow obtaining the resultant net magnetic field and torque acting on the internal rotor unit by multiple sources of magnetic field.

2 System Modelling

In this section, the model for a single coil-single rotor system is defined. The relationship of the electromagnetic coil actuation (input: current to the coil) to the generated magnetic field at an arbitrary location (representing the location of the internal rotor unit) is derived in Section 2.2. The relationship of the resultant magnetic field at the given location to the generated wrench acting on the internal rotor unit (as the result of the magnetic flux linkage with the permanent magnet of the rotor) is presented in Section 2.3. The case of having multiple sources of magnetic field on a single permanent magnet rotor is briefly summarised in this section using the *Principle of Superposition*.

2.1 Model Definition

The single coil-single rotor model in consideration for this study is as illustrated in Figure 1. This represents the most general case model of the proposed LEMA concept, representing a stator-rotor pair, where the stator is the external electomagnetic coil representing a source of magnetic field actuated by our system input while the rotor is a permanent magnet internal rotor unit. The final system may be constructed out of two electromagnetic coils as the stator, however the principle of superposition could simply be applied, as will be shown in this paper. The overall system will therefore have n stator-rotor sets (i = 1,2,...,n). The internal device (deployed through the surgical port into the abdominal cavity) is anchored to the abdominal wall by the coupling of the internal and external anchoring magnets, i.e. Ai_i and Ae_i, respectively. The stator coils, S_i are actuated by the input current, I_i which produce magnetic field (B_i) across the abdominal wall which generate wrench acting on the corresponding permanent magnet internal rotor unit (rotor i). The stator coils, S_i and the external anchoring magnets, Ae_i are assumed to be rigidly fixed to an external platform such that its weight is not resting upon the abdominal wall. The model with the notations are summarised in Figure 2.

2.2 Magnetic Field Model

The magnetic field produced by an electromagnetic coil S_i measured an arbitrary point $P(x,y,z)$ is modelled based on

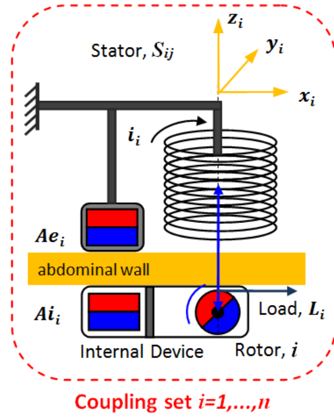

Figure 2: i^{th} coupling set of the simplified system where j caters for multiple stator coils

the Biot-Savart Law [Furlani *et al.*, 2001] (Figure 3) and is presented as:

$$B_q = \frac{\mu_0 \mu_r I N R_c}{4\pi} \int_{z'=l/2}^{l/2} \int_{\varphi'=0}^{2\pi} \frac{C_q}{D} d\varphi' dz' \qquad (1)$$

where $q = x, y$, and z, respectively, μ_0 and μ_r are the permeability of free space ($4\pi \times 10^7 H/m$) and the relative permeability of the core material, respectively, R_c is the radius of the coil, N is the number of turns in the coil and

$$C_q = \begin{cases} (z\text{-}z')\cos\varphi'\hat{i}, & q = x \\ (z\text{-}z')\sin\varphi'\hat{j}, & q = y \\ (R - x\cos\varphi' - y\sin\varphi')\hat{k}, & q = z \end{cases}$$

$$D = (x^2 + y^2 + (z\text{-}z')^2 + R_c^2 - 2R_c(x\cos\varphi' + y\sin\varphi'))^{3/2} \qquad (2)$$

The resultant magnetic field, $B \in \Re^3$ on an arbitrary point P is given by:

$$B = B_x\hat{i} + B_y\hat{j} + B_z\hat{k}. \qquad (3)$$

This magnetic field model is applicable to the case of multiple electromagnetically generated fields, e.g. the case of having multiple stator coils for one rotor and the disturbance produced by the other stator/rotor sets in the vicinity, through *Principle of Superposition*. The resultant magnetic field is obtained as the vector sum of the magnetic fields contributed by the multiple magnetic sources at point P [Furlani *et al.*, 2001]. The resultant magnetic field, B is then obtained from Equations 3 as discussed and will be utilized in the electromechanical model in the following subsection to determine the dynamics of the system.

2.3 Modelling of Flux Linkage Generated Wrench

The resultant magnetic field, B at Point P is essential for the analysis of the system dynamics. Following the Newton-Euler approach, the free body diagram of the permanent magnet internal rotor unit, given in Figure 4 shows the forces and

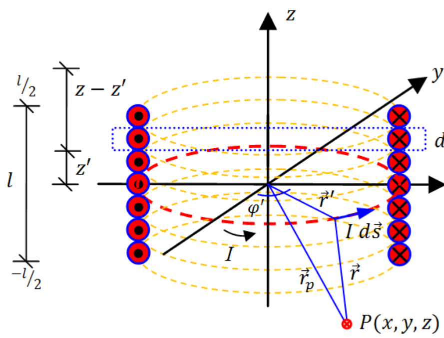

Figure 3: An arbitrary point, *P(x,y,z)* around an electromagnetic coil

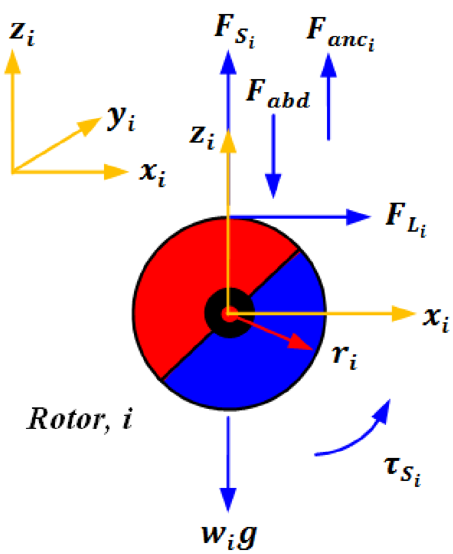

Figure 4: Free body diagram of the i^{th} rotor in consideration

moments acting on it in all directions in 3D space. Without the loss of generality, the analysis is performed on rotor i, as depicted in Figure 2.

The Case of Single Stator Coil

Note that the intended motion in the system is the rotation of the permanent magnet rotor i.. The other 5 DOFs of the permanent magnet rotor i are ideally rigidly constrained. However, in practice, this may not be the case, and the modelling effort in this paper takes into account the forces and moments acting in these directions, through the Newton-Euler approach of rigid body modelling. Example of forces in the direction of constraints are those exerted by the viscoelastic nature of the insufflated abdominal wall and by the anchoring magnets. While these components are not explored in depth in this paper, the modelling effort allows them to be accommodated in future studies.

As the stator coil and the external permanent magnet anchor are attached to an external platform, the force of the anchoring magnet, F_{anc_i} is required to be sufficiently large to overcome the weight of the internal rotor unit which is holding the internal permanent magnet anchor and rotor i at all times. The lateral effect of the internal permanent magnet anchor onto the rotor is assumed negligible with the presence of the shielding material in between the anchor and rotor within the internal device housing.

With the body attached coordinate frame as defined in Figure 4, the forces acting on the rotor i can be summarised as:

$$\sum F = F_{S_i} + F_{anc_i} + F_{abd} + F_{L_i} - w_i g. \tag{4}$$

where w_i is the mass of the assembly of internal device, r_i is the radius of the corresponding rotor, $F_{anc_i} \in \Re^3$ is the force exerted by the anchoring permanent magnets, which is assumed to have only component in the z_i direction, and $F_{L_i} \in \Re^3$ is the load. $F_{abd} \in \Re^3$ is the force acting on the permanent magnet rotor i due to the abdominal wall, which could be modelled as a spring and damper system:

$$F_{abd} = \begin{bmatrix} 0 \\ 0 \\ k_{abd} z + b_{abd} \dot{z} \end{bmatrix} \tag{5}$$

and $F_{S_i} \in \Re^3$ is the force generated by the stator magnetic field and is given by:

$$F_{S_i} = (m_i \bullet \nabla) B_i \tag{6}$$

where $m_i \in \Re^3$ is the magnetic moment of the permanent magnet rotor i, which is related to the magnetization $M_i \in \Re^3$ and the length of the rotor, h_i, given by:

$$m_i = \pi r_i^2 h_i M_i \tag{7}$$

It should be noted that F_{S_i} is the attraction / repulsion forces on the rotor, in the direction of constraint, caused by the stator. If the internal rotor unit is perfectly aligned to the centre of the magnetic field generated by the stator, then it would only have non-zero components in the z_i direction. It does not contribute to the desired actuation, which is the torque about the rotor axis.

Similarly, the torque on permanent magnet rotor i is given as follows:

$$\sum \tau_i = J_i \ddot{\theta}_i + b_i \dot{\theta}_i = \tau_{S_i} - \tau_{L_i} \tag{8}$$

where $J_i \in \Re^{3\times3}$ and $b_i \in \Re^{3\times3}$ are the total moment of inertia and the viscous friction coefficient of the permanent magnet rotor respectively, and $\theta_i \in \Re^3$ is the rotation position of the rotor about each axis. The torque on the permanent magnet rotor by the electromagnet, $\tau_{S_i} \in \Re^3$ and the load torque, $\tau_{L_i} \in \Re^3$ are expressed as:

$$\begin{aligned} \tau_{S_i} &= m_i \times B_i = \begin{bmatrix} -B_y m_i \cos\theta \\ -B_z m_i \sin\theta - B_x m_i \cos\theta \\ -B_y m_i \sin\theta \end{bmatrix} \\ \tau_{L_i} &= r_i \times F_{L_i} \end{aligned} \tag{9}$$

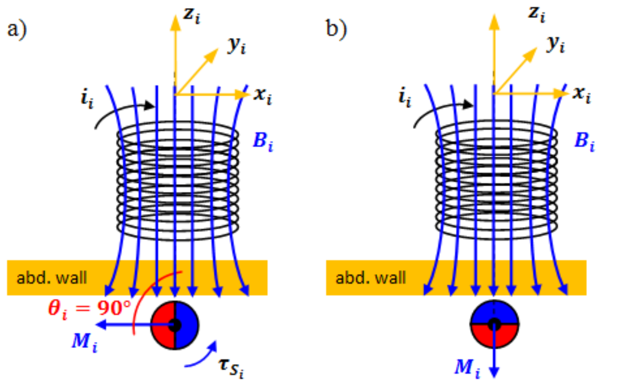

Figure 5: (a) Maximum τ_{S_i} obtained at M_i at 90 degrees angle from the direction of B_i, and b) zero torque when M_i is aligned with B_i

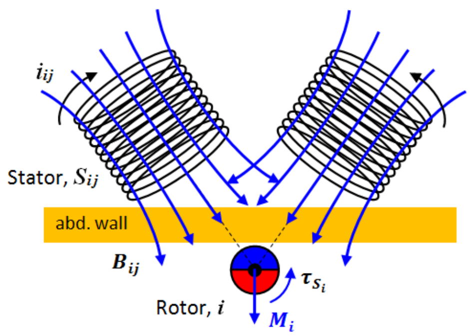

Figure 6: The net torque, τ_i resulted from the superposition of the magnetic fields generated by stator coils, S_{ij} $(j = 1, 2)$

When the angular displacements (misalignment) about x and z axes are zero (i.e. when the permanent magnet rotor is rigid and well aligned with the stator), Equations 8 and 9 simplify to:

$$\sum \tau_i = J_i \ddot{\theta}_i + b_i \dot{\theta}_i = \tau_{S_i} - r_i F_{L_i}$$
$$\text{where} \quad \tau_{S_i} = m_i \times B_i = \pi r_i^2 h_i M_i B_i \sin^2(\theta_i) \tag{10}$$

In order to analyse the maximum static torque produced by a coil S_i on the generated torque on rotor i, the direction of the magnetization of the rotor, M_i has to be at 90 degrees to the direction of the stator magnetic field at the point of evaluation B_i (as illustrated in Figure 5). When the M_i is parallel to B_i, zero torque is produced on rotor i, the rotor will not rotate. In these scenarios, the generated force on the rotor will be purely attractive or repulsive. This is an important consideration for the design of the system, which is reflected in the simulations and experiments discussed in the following sections.

The Case of Multiple Stator Coils

In the presence of N_s (multiple) stator coils, the torque generated on rotor i (τ_{S_i}) can be summed up by the *Principle of Superposition* as:

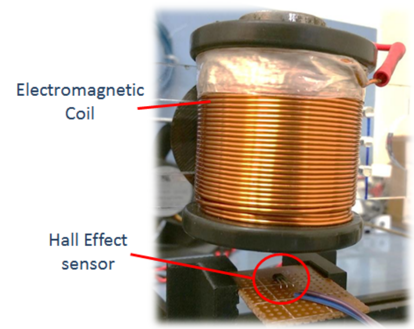

Figure 7: The Hall Effect sensor (circled in red) used to measure the magnetic field contributed by the electromagnetic coil, at the rotor position

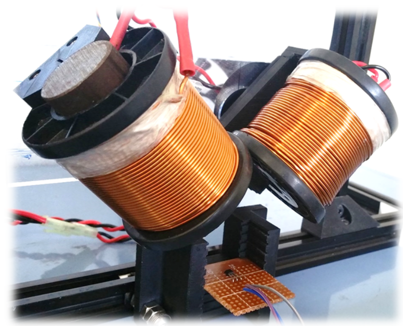

Figure 8: An additional coil is added to the setup to verify the assumption of the resultant magnetic fields at a given point in space generated by multiple sources follow the principle of superposition

$$\sum \tau_{S_i} = \sum_{j=1}^{N_s} (m_i \times B_{ij}) \tag{11}$$

where $j = 1, 2, ..., N_s$ is the number of magnetic sources contributing to the torque onto rotor i. The case of having two stator coils (ie. $N_s = 2$) is shown in Figure 6.

3 Experimental Setup

To validate the mathematical models described in Section 2, an experimental setup is constructed to facilitate two sets of experimental measurements, as described in the subsections below.

3.1 Setup for Magnetic Field Model Validation

The first setup comprises an electromagnetic coil as the stator and a Hall effect sensor (UGN3503UA) as shown in Figure 7. In this setup, we are able to measure the resultant B in terms of Gauss, G (i.e. 1G$= 1 \times 10^{-4}$T) as contributed by the electromagnet coil at the given rotor location. The magnetic field, B is measured at various inter-magnetic distances below the stator coil (i.e. 20mm, 30mm, 40mm and 50mm), generated by input constant input current ranging from -5A to $+5$A, to validate that the mathematical model provides an accurate magnetic field result with different current conditions. The different inter-magnetic distances simulates the variations in the abdominal wall thickness separating the stator and the rotor, starting at 20mm away representing a slim patient, with average patient measuring 30-40mm in abdominal wall thickness. The magnetic field B at the rotor position in the horizontal, x-direction (i.e. from the centre of the coil, 0mm up to 80mm away from the coil) is also measured to observe the effect of the magnetic field generated by the stator onto the rotor at lateral offset positions.

Magnetic field superposition is tested by placing two stator coils side by side and turning on one coil at a time (see Figure 8) and both coils simultaneously. The x and z components (with zero lateral offset in y axis) of the magnetic field are measured using the Hall Effect sensor. These values obtained will be compared with the values simulated for validation in Section 5.

3.2 Setup for Magnetic flux Generated Torque Validation

The second setup comprises the same electromagnetic stator and a permanent magnet rotor (in place of the Hall Effect sensor in the first setup). This setup is intended to validate the relationship between the input current to the stator coil(s) and the output torque about the rotor. To measure the torque transmitted by the electromagnetic coil onto the permanent magnet rotor (τ_{S_i}), the rotor is attached to a torque sensor (ATI F/T Gamma), as shown in Figure 9. The rotor is fixed in its orientation with its magnetization (i.e. direction of south to north) at 90deg from the centre axis of the electromagnet to produce the maximum static torque, as illustrated in Figure 5a. The electromagnet stator is supplied with a constant DC current ranging from -5A to $+5$A. The torque sensor then measures the static torque acting on the rotor at different distance settings in the x and z directions, as explained in Section 3.1. The static torque measurements along the horizontal x direction allows the observation of the torque onto the rotor at an offset position away from the centre of the stator and the measurements along the z-axis simulate the static torque experienced by the rotor at different abdominal wall thickness.

A two-stator coil scenario is also set up to validate the accuracy of the principle of superposition on the torque onto the rotor. The coils are alternately turned on for individual τ_{S_i} measurements and then both coils are turned on simultaneously to obtain the resultant τ_{S_i} value.

4 Parameter Identification

Several parameters of the physical setup need to be identified for the purpose of the numerical simulation and its comparison to the experimental results. These parameters are the relative permeability of the electromagnet core, μ_{r_i} in the magnetic model (Equation 1) and the value of the magnetization of the permanent magnet rotor, M_i, in the electromechanical model (Equation 10).

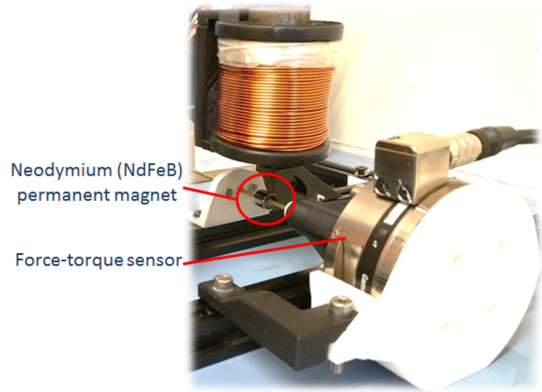

Figure 9: A force-torque sensor is used to measure the torque generated by the coil onto the permanent magnet rotor

To determine the relative permeability of the electromagnet core μ_{r_i}, the magnetic field generated by the coil is measured with and without the iron core. The difference between the two readings is the compensated value for the particular μ_{r_i}. Even though the ferromagnetic core displays non-linear hysteresis in the B-H curve, the system is assumed to operate within the linear operating region. Note that B and H refer to the flux density and field strength, respectively. As the stator core is customized independently to fit into each coil, the permeability of each core is expected to be slightly different and this identification method can be repeated for other electromagnetic coils to obtain the specific μ_{r_i}. In this case, the relative permeability of the stator coil is identified to be, $\mu_{r_i} = 5.2$.

Following the measurement of μ_{r_i}, the flux density B_i is obtained from Equation 3. The generated rotor torque τ_{S_i} due to B_i can be measured using a force torque sensor (elaborated in Section 3) for a given rotor angular displacement θ from Equations 10 and 11 (for the case with multiple stators). The magnetization, M_i is dependent on factors such as the size and the shape of the permanent magnet and this is usually simulated numerically using finite element methods. Nonetheless, for the purpose of the parameter identification, M_i can now be obtained from Equation 10, as all other variables are measured or known. The static torque measurements obtained in Section 3 yielded an average value of $M_i = 4.45 \times 10^5$ A/m for the stator coil used in this experiment.

5 Model Validations

The magnetic field model and the magnetic flux linkage generated torque models discussed in Section 2 are implemented in numerical simulations, with the parameters identified from an experimental setup. The results are then validated against an independent set of experimental measurements to evaluate

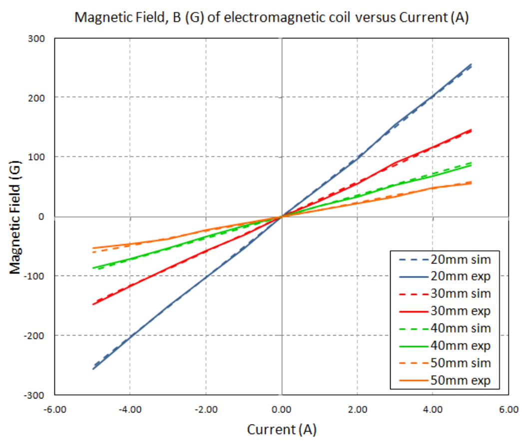

Figure 10: Comparison between simulated and experimental results of B from electromagnetic stator measured at 20mm to 50mm along z-axis simulating the varying abdominal wall thickness(separation distance between stator coil and rotor). The horizontal axis represents the input current to the stator coil.

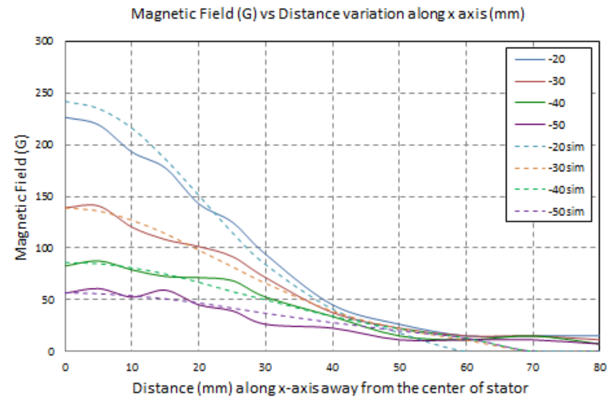

Figure 11: Comparison between simulated and experimental results of B, measured at abdominal wall thicknes (distance in z axis between stator and rotor) of 20mm to 50mm. The horizontal axis represents the lateral misalignment of the rotor from the centre of the stator coil at 10mm intervals.

the accuracy of the model. The simulations and experiments are carried out on a single (stator) coil and a single rotor configuration for the simplicity of the validation without loss of generality.

The validation process involves simulations and experimental measurements of magnetic field, B with a variation along the z-axis (simulating the different abdominal wall thicknesses that contribute to the inter-magnetic distance between the stator and rotor) as well as the variations along the horizontal x-axis (simulating the lateral offset of the rotor from the centre of the coil upon intra-abdominal deployment) versus current.

The second part of the process utilises the B values obtained from the earlier magnetic model validation to numerically compute the static torque in the simulation for validation against the static torque measured experimentally. The experiment was also performed with the rotor placed 20mm to 50mm below the stator in the z-axis to visualise the inter-magnetic distance due to the abdominal wall thickness versus the variations along the x-axis to observe the stator torque onto the rotor when it is misaligned from the centre of the stator coil.

5.1 Simulations

Simulations of the models described in Section 2 are performed for the case of single coil-single rotor system to observe the computed numerical responses of the system in MatLab and its comparison to the experimentally measured response described in Section 3. The parameters $\mu_r = 5.2$ and $M = 4.45 \times 10^5$ identified in Section 4 are employed into the magnetic and electromechanical models to simulate the magnetic field, B as well as the torque, τ onto the rotor at any point in the workspace generated by a single coil.

The results of the magnetic field with z-axis inter-magnetic distance and x-offset variations are plotted along with the experiment data obtained from the experimental procedures (refer tp Section 3) in Figures 10 and 12, respectively.

5.2 Magnetic Field Model Validation

The magnetic field readings B, measured using the Hall Effect sensor as described in Section 3.1 are presented along with the Matlab simulated values in Figures 10 and 11 with respect to current (A) to validate the accuracy of the numerical model with respect to the actual measurements. The comparison shows a close fit between the theoretical model and the actual experimental measurements, taken at different locations of the rotor, simulating different inter-magnetic distances due to various abdominal wall thickness (Figure 10) and at different values of lateral offset (Figure 11), simulating possible misalignment in the practical setup. Towards further x-offset (i.e. 60mm onwards away from the centre of the coil), the magnetic field is ideally zero in simulation. It is not ideal in the actual experiment as the Hall Effect sensor is prone to measurement noises in the environment. Nonetheless, these measurement discrepancies are considered negligible in term of its unit in Gauss. The model accuracy will greatly aid in the electromechanical analysis of the torque produced onto the rotor in Section 5.3.

5.3 Magnetic Flux Generated Torque model Validation

The results obtained from the numerical computation of the resultant rotor torque, obtained from the magnetic flux generated torque model in Section 2.3 are validated against the torque values measured experimentally using the torque sensor. These simulation and experiment are also performed with the variations in the z and x directions, simulating the stator-rotor inter-magnetic separation due to different abdominal wall thickness and stator-coil misalignment, respectively. This allows the observation of the rotor behaviour with the given torque at any possible intra-abdominal deployment positions. Figure 12 shows the comparison between the simulated and measured torque. The results show good fit with some noise observed. The torque onto the rotor decreases exponentially along the x-direction. This information is important for the design specification so accurate intra-abdominal placement of the rotor can be taken into consideration. Nevertheless, with position guidance and anchoring of the internal device with permanent magnet anchors, the possibility of the rotor being misaligned with the centre of the coil beyond 20mm offset can be reduced, thus minimizing the loss of torque onto the rotor.

5.4 Magnetic Field and Torque Superposition

For the case of having two stator coils, the simulation and experimental measurements are executed according to the procedures described in Section 3. The magnetic field values are presented and compared in Table 1. It is shown that the principle of superposition are accurate in accounting for the use of two stator coils in the resultant magnetic field.

Table 1: Validation of magnetic field superposition

Stator, S_i Status	B_x component (G) Exp	Sim	B_z component (G) Exp	Sim
S_1 on, S_2 off	78.95	77	-146.62	-148
S_1 off, S_2 on	75.19	77	146.62	148
S_1 on, S_2 on	154.14	153	-15.04	0

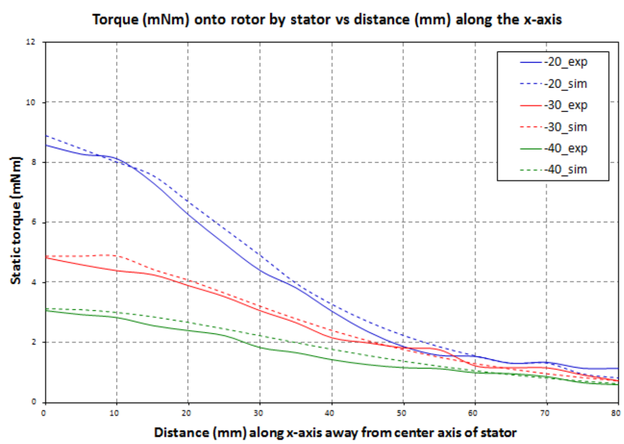

Figure 12: Comparison between simulated and experimental results of τ_1 generated by the stator onto the rotor measured at 20mm to 50mm vertical inter-magnetic distances and 0mm to 80mm lateral distances from the centre of the coil (x-offset).

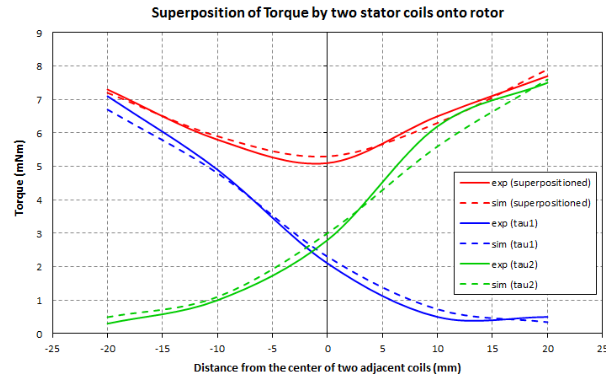

Figure 13: Comparison between simulated and experimental results of superpositioned τ_2 from both stator 1 and stator 2

Similarly, the principle of superposition of the generated rotor torque by the two stator coils is tested. The superposition B values obtained in the manner described above are also used to validate the computationally produced static superposition torque, τ_{S_i} onto the rotor with the values measured by the ATI torque sensor. The plots for both the simulations and experimental results are presented in Figure 13. The torque measured when only stator coil 1 is on is labelled as tau1, represented with the blue lines, while the torque measured when only coil 2 was turned on is labelled as tau2, represented with the green lines. The resultant torque contributed by both the coils, is represented by the red lines (Figure 13). The result conforms to the summation of the torque from the individual coils.

6 Conclusion and Future Work

The model of system dynamics in the form of magnetic field model and and the model of the magnetic flux generated wrench for the LEMA system is presented. This is a fundamental and essential step to the design and performance analyses as well as the implementation of the system as it enables the contributions of various sources of magnetic fields as well as the dynamics of the physical and environmental uncertainties in the vicinity of the rotor to be taken into consideration. The validation of the models provides a strong platform for future work which includes the establishment of the design specifications for the LEMA system as well as the development of controllers to reject external disturbances onto the corresponding rotor and to achieve desired speed or torque accurately for surgical manipulations.

References

[Leong *et al.*, 2016] F. Leong, N. Garbin, C. Di Natali, A. Mohammadi, D. Thiruchelvam, D. Oetomo, and P. Valdastri. Magnetic surgical instruments for robotic abdominal surgery. *IEEE Reviews on Biomedical Engineering*, 2016.

[Richardson *et al.*, 2000] W. S. Richardson, K. M. Carter, G. M. Fuhrman, J. S. Bolton, and J. C. Bowen. Minimally invasive abdominal surgery. *The Ochsner Journal*, 2(3), 153-157, 2000.

[Cadeddu *et al.*, 2009] J. Cadeddu, R. Fernandez, M. Desai, R. Bergs, C. Tracy, S. J. Tang, P. Rao, M. Desai, and D. Scott. Novel magnetically guided intra-abdominal camera to facilitate laparoendoscopic single-site surgery: initial human experience. *Surgical Endoscopy.* 23(8), 1894-1899, 2009.

[Park *et al.*, 2007] S. Park, R. A. Bergs, R. Eberhart, L. Baker, R. Fernandez, and J. A. Cadeddu. Trocar-less instrumentation for laparoscopy: magnetic positioning of intra-abdominal camera and retractor. *Annals of surgery.* 245(3), 379–384, 2007.

[Tortora *et al.*, 2013] G. Tortora, M. Salerno, T. Ranzani, S. Tognarelli, P. Dario, and A. Menciassi. A modular magnetic platform for Natural Orifice Transluminal Endoscopic Surgery (NOTES). *In Procs. IEEE International Conference of Engineering in Medicine and Biology Society (EMBS).* 6265-6268, 2013.

[Vartholomeos *et al.*, 2013] P. Vartholomeos, C. Bergeles, L. Qin, and P. E. Dupont. An MRI-powered and controlled actuator technology for tetherless robotic interventions *The International Journal of Robotics Research* 32(13), 1536–1552, 2013.

[Kummer *et al.*, 2010] M. P. Kummer, J. J. Abbott, B. E. Kratochvil, R. Borer, A. Sengul, and B. J. Nelson. OctoMag: An electromagnetic system for 5-DOF wireless micromanipulation. *IEEE Transactions on Robotics* 26(6), 1006–1017, 2010.

[Munoz *et al.*, 2015] F. Munoz, G. Alici, and W. Li. Optimization of multiple arc-shaped magnets for drug delivery in a capsule robot *In Procs. IEEE International Conference on Advanced Intelligent Mechatronics (AIM)* 189–195, 2015.

[Carpi *et al.*, 2009] F. Carpi, and C. Pappone. Stereotaxis Niobe magnetic navigation system for endocardial catheter ablation and gastrointestinal capsule endoscopy *Expert Review of Medical Devices* 6(5), 487–498, 2009.

[Di Natali *et al.*, 2015] C. Di Natali, J. Buzzi, N. Garbin, M. Beccani, and P. Valdastri. Closed-loop control of local magnetic actuation for robotic surgical instruments *IEEE Transactions on Robotics* 31(1), 143–156, 2015.

[Hang *et al.*, 2015] G. Hang, M. Bain, J. Y. Chang, S. Fang, F. Leong, A. Mohammadi, P. Valdastri, and D. Oetomo. Local Magnetic Actuation Based Laparoscopic Camera for Minimally Invasive Surgery. Australasian Conference on Robotics and Automation (ACRA), 2015.

[Mohammadi *et al.*, 2015] C. Di Natali, A. Mohammadi, D. Oetomo, and P. Valdastri. Surgical Robotic Manipulator Based on Local Magnetic Actuation. *Journal of Medical Devices* 9(3), 090336, 2015.

[Mohammadi *et al.*, 2015] A. Mohammadi, C. Di Natali, D. Samsonas, P. Valdastri, Y. Tan, and D. Oetomo. Electromagnetic Actuator Across Abdominal Wall for Minimally Invasive Robotic Surgery. *Journal of Medical Devices* 9(3), 030937, 2015.

[Mohammadi *et al.*, 2015] A. Mohammadi, D. Samsonas, C. Di Natali, P. Valdastri, Y. Tan, and D. Oetomo. Speed control of non-collocated stator-rotor synchronous motor with application in robotic surgery. *in Procs. 10th Asian Control Conference* 31 May - 3 June 2015, pp 1-6.

[Furlani *et al.*, 2001] E. P. Furlani. Permanent magnet and electromechanical devices: materials, analysis, and applications. *Academic Press*, 2001.